Editors' Suggestion

Nonreciprocal Phonon Laser

Y. Jiang,[1] S. Maayani,[2] T. Carmon,[2] Franco Nori,[3,5] and H. Jing[4,*]

[1] *Department of Physics, Henan Normal University, Xinxiang 453007, China*
[2] *Mechanical Engineering, Technion—Israel Institute of Technology, Haifa 32000, Israel*
[3] *Theoretical Quantum Physics Laboratory, RIKEN Cluster for Pioneering Research, Wakoshi, Saitama 351-0198, Japan*
[4] *Department of Physics and Synergetic Innovation Center for Quantum Effects and Applications, Hunan Normal University, Changsha 410081, China*
[5] *Physics Department, The University of Michigan, Ann Arbor, Michigan 48109-1040, USA*

(Received 10 June 2018; revised manuscript received 30 November 2018; published 14 December 2018)

We propose nonreciprocal phonon lasing in a coupled cavity system composed of an optomechanical resonator and a spinning resonator. We show that the optical Sagnac effect leads to significant modifications in both the mechanical gain and the power threshold for phonon lasing. More importantly, the phonon lasing in this system is unidirectional; that is, the phonon lasing occurs when the coupled system is driven in one direction but not the other. Our work establishes the potential of spinning optomechanical devices for low-power mechanical isolation and unidirectional amplification. This provides a new route, well within the reach of current experimental abilities, to operate cavity optomechanical devices for a wide range of applications such as directional phonon switches, invisible sound sensing, and topological or chiral acoustics.

DOI: 10.1103/PhysRevApplied.10.064037

I. INTRODUCTION

Cavity optomechanical (COM) [1–3] is playing an increasingly important role in making and steering on-chip devices, such as long-lived quantum memory [4], transducers [5–7], motion-sensing devices [8–10], and phonon lasers [11–18]. Phonon lasing, or coherent mechanical amplification, exhibits properties similar to those of an optical laser, such as threshold, gain saturation, and linewidth narrowing in the lasing regime [19–22], as demonstrated in experiments with trapped ions, nanobeams, superlattices, resonators, or electromechanical devices [11–18]. It provides coherent acoustic sources to drive phononic devices for practical applications in, for example, audio filtering, acoustic imaging, and topological sound control [23–27]. COM-based ultralow-threshold phonon lasers, featuring a continuously tunable gain spectrum to selectively amplify phonon modes, from radio-frequency to microwave rates [16–18], provide a particularly attractive setting to explore quantum acoustic effects, such as two-mode mechanical correlations [14] or phononic sub-Poissonian distributions [15].

In parallel, nonreciprocal optics [28,29] has emerged as an indispensable tool for a wide range of applications such as invisibility cloaking, noise-free sensing, directional lasing, and one-way optical communications [30–35]. Directional transmission of light has been achieved with optical nonlinearities or dynamically modulated media [36–43]. As a crucial element in signal read-out and information processing, directional optical amplifiers (with minimal noise from the output port) have also been proposed and studied in microwave circuits [44,45] and a non-Hermitian time-Floquet device [46]. In a recent experiment, a reconfigurable optical device was demonstrated [47], having switchable functions as either a circulator or a directional amplifier [48,49]. Directional amplification of microwave signals has also been experimentally demonstrated in a multimode COM system [50]. These abilities, allowing directional transmission and amplification of optical signals [51–55], are fundamental for the emerging fields of chiral quantum optics and topological photonics [56].

As in optical systems [44–49], directional emission and amplification of phonons are particularly important in mechanical engineering [57–66], such as acoustic sensing or computing [23–26]. Here we propose a strategy to achieve a *nonreciprocal mechanical amplifier* by coupling a COM resonator to a purely optical spinning resonator. We show that by exploiting the optical Sagnac effect [67–69], we can significantly alter both the mechanical gain and the phonon-lasing threshold. In particular, by driving of the COM resonator from the left or the right side, coherent

*jinghui73@foxmail.com

emission of phonons is enhanced or completely suppressed, realizing a highly tunable nonreciprocal phonon laser. This provides a key element for applications of COM devices in, for example, chiral quantum acoustics or topological phononics [25,26].

Very recently, by the spinning of a whispering-gallery-mode (WGM) optical resonator, nonreciprocal transmission with 99.6% rectification was observed for photons, without any magnetic field or optical nonlinearity [70]. By the spinning of a shape-deformed resonator, purely optical effects such as mode coupling [71] and broken chiral symmetry [72] have also been revealed. Such spinning devices can also be useful in nanoparticle sensing [73] or single-photon control [74]. For sound, excellent isolation was demonstrated even earlier by use of a circulating fluid [75]. In recent experiments, chiral mechanical cooling was realized via nonreciprocal Brillouin scattering [58,62–64]. Here, as another necessary element, we show that nonreciprocal *amplification* of phonons can be achieved by use of the optical Sagnac effect induced by a spinning resonator [70]. This opens up a new route to operate nonreciprocal COM devices for applications in, for example, backaction-immune force sensing [11] and chiral acoustic engineering [76,77].

II. MODEL AND SOLUTIONS

We consider two coupled resonators, one of which is purely optical and the other supports a mechanical breathing mode (frequency ω_m and effective mass m) when pumped by light of frequency ω_L and amplitude ε_L. Evanescent coupling between these resonators exists in the 1550-nm band, and the laser is coupled into and out of the resonator via a waveguide (see Fig. 1). The two resonators share the same resonance frequency ω_c for the stationary case. The decay rates of the COM resonator and the optical resonator are γ_1 and γ_2, respectively, which are related to the optical quality factors Q_1 and Q_2 (i.e., $\gamma_{1,2} = \omega_c/Q_{1,2}$). This compound system, used to observe phonon lasing experimentally [16,17], can be further tuned by spinning of the optical resonator with speed Ω, due to the Ω-dependent optical Sagnac effect. An immediate consequence of this effect is that for the counterclockwise (CCW) rotation denoted by $\Omega > 0$, *phonon lasing can be enhanced or blocked* by driving of the system from the left or the right [or equivalently, for the clockwise (CW) rotation denoted by $\Omega < 0$, the phonon lasing is enhanced by driving of the system from the right and it is blocked when the driving is from the left]. This, as already mentioned, realizes a *highly tunable nonreciprocal phonon laser* by flexible tuning of the rotation speed and the drive direction.

In a spinning resonator, the CW or CCW optical mode experiences different refractive indices [70]; that is, $n_\pm = n[1 \pm r_2\Omega(n^{-2} - 1)/c]$, where n and r_2 denote, respectively, the refractive index and the radius of the resonator,

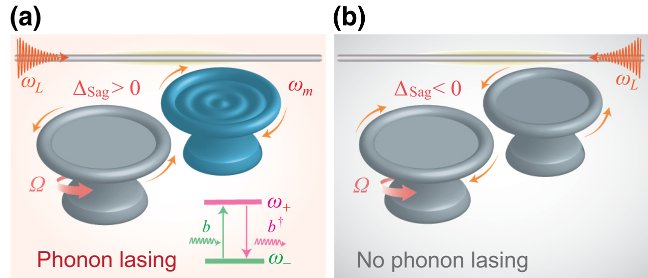

FIG. 1. (a) A nonreciprocal phonon laser composed of a spinning optical resonator coupled to a COM resonator. For the CCW rotation, driving of the system from the left (with $\Delta_{\rm Sag} > 0$) increases the mechanical gain. The inset shows the equivalent two-level-system model for phonon lasing where the transitions between supermodes are mediated by phonons. (b) Driving the system from the right (with $\Delta_{\rm Sag} < 0$) suppresses or even completely blocks the phonon-lasing process.

and c is the speed of light in vacuum. As a result, the frequencies of the CW and CCW modes of the resonator experience Sagnac-Fizeau shifts [78,79]. For light propagating in the same direction as, or direction opposite that of, the spinning resonator, we have

$$\omega_c \to \omega_c \mp |\Delta_{\rm Sag}|,$$

with

$$\Delta_{\rm Sag} = \pm\Omega\frac{nr_2\omega_c}{c}\left(1 - \frac{1}{n^2} - \frac{\lambda}{n}\frac{dn}{d\lambda}\right), \tag{1}$$

where $\lambda = c/\omega_c$ is the optical wavelength. The dispersion term $(\lambda/n)(dn/d\lambda)$ denotes the Lorentz correction to the Fresnel-Fizeau drag coefficient, characterizing the relativistic origin of the Sagnac effect [78]. This term, which is relatively small in typical materials, can be safely ignored as confirmed in a recent experiment [70]. In such a device, light is dragged by the spinning resonator, leading to nonreciprocal transmissions for optical counterpropagating modes (see Ref. [70] for more details). Below we show that for our COM system this leads to distinct changes of the radiation pressure on the mechanical mode, hence resulting in a *nonreciprocal phonon laser*.

As shown in Fig. 1, spinning the resonator along the CCW direction and driving the device from the left or the right induce an optical redshift or blueshift (i.e., $\Delta_{\rm Sag} > 0$ or $\Delta_{\rm Sag} < 0$). The Hamiltonian of the system, in a frame rotating at frequency ω_L, can be written as ($\hbar = 1$)

$$\begin{aligned} H &= H_0 + H_{\rm int} + H_{\rm dr}, \\ H_0 &= -\Delta_L a_1^\dagger a_1 - (\Delta_L + \Delta_{\rm Sag}) a_2^\dagger a_2 + \omega_m b^\dagger b, \\ H_{\rm int} &= -\zeta x_0 a_1^\dagger a_1 (b^\dagger + b) + J(a_1^\dagger a_2 + a_2^\dagger a_1), \\ H_{\rm dr} &= i(\varepsilon_L a_1^\dagger - \varepsilon_L^* a_1). \end{aligned} \tag{2}$$

H_0 is the free Hamiltonian, where the first and second terms describe the optical modes in the COM resonator and the spinning resonator, respectively, and the third term denotes the energy of the mechanical mode. $H_{\rm int}$ is the interaction Hamiltonian, where the first term describes the coupling between the optical and mechanical mode in the optomechanical resonator and the second term describes the coupling between the optical modes of the resonators. $\Delta_L = \omega_L - \omega_c$ is the detuning between the drive laser and the resonance frequency of the resonator, a_1 and a_2 denote the optical annihilation operators of the resonators (coupled with the optical strength J), $x_0 = \sqrt{\hbar/2m\omega_m}$, b is the mechanical annihilation operator, $\zeta = \omega_c/r_1$ denotes the COM coupling strength, and r_1 is the radius of the COM resonator. Finally, $H_{\rm dr}$ denotes the drive that is fed into the coupled-resonator system through the waveguide (see Fig. 1), with driving amplitude

$$\varepsilon_L = \sqrt{2\gamma_1 P_{\rm in}/\hbar\omega_L}$$

and input power $P_{\rm in}$.

The Heisenberg equations of motion of this compound system are then written as

$$\begin{aligned}\dot{a}_1 &= (i\Delta_L - \gamma_1)a_1 + i\zeta x_0(b+b^\dagger)a_1 - iJa_2 + \varepsilon_L,\\ \dot{a}_2 &= [i(\Delta_L + \Delta_{\rm Sag}) - \gamma_2]a_2 - iJa_1,\\ \dot{b} &= -(i\omega_m + \gamma_m)b + i\zeta x_0 a_1^\dagger a_1,\end{aligned} \tag{3}$$

where γ_m is the damping rate of the mechanical mode. As already confirmed in an experiment with an optomechanical phonon laser [16], for a strong pump field, the quantum noise terms can be safely ignored if one is interested only in the mean-number behaviors (i.e., the threshold feature of the mechanical gain or the phonon amplifications). Setting all the derivatives of Eq. (3) to zero, we can readily derive the steady-state solutions of the system as

$$\begin{aligned}a_{1,s} &= \frac{\varepsilon_L}{\gamma_1 - (i\Delta_L + \zeta x_s) + J^2/[\gamma_2 - i(\Delta_L \pm |\Delta_{\rm Sag}|)]},\\ a_{2,s} &= \frac{Ja_{1,s}}{\Delta_L \pm |\Delta_{\rm Sag}| + i\gamma_2}, \quad b_s = \frac{\zeta x_0 |a_{1,s}|^2}{\omega_m - i\gamma_m},\end{aligned} \tag{4}$$

where $x_s = x_0(b_s + b_s^*)$ is the steady-state mechanical displacement. Combining these expressions gives the balance equation of the radiation and spring forces:

$$m(\omega_m^2 + \gamma_m^2)x_s = \hbar\zeta|a_{1,s}|^2.$$

The displacement x_s is determined from the optical density $|a_{1,s}|^2$ inside the COM resonator, which clearly depends on $\Delta_{\rm Sag}$ (see also Fig. 2; e.g., both $|a_{1,s}|^2$ and x_s become significantly different for $\Delta_{\rm Sag} > 0$ or $\Delta_{\rm Sag} < 0$). Also, the

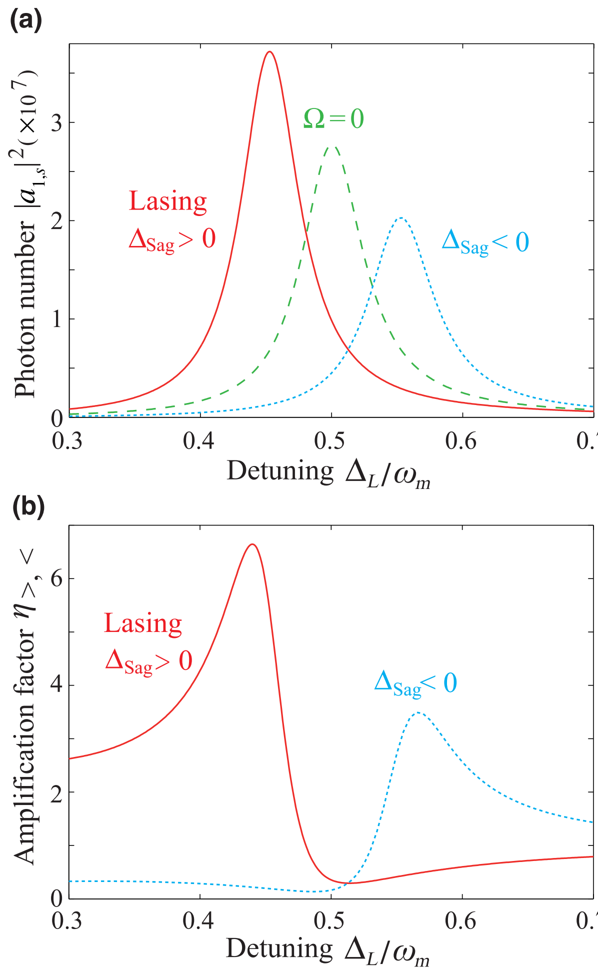

FIG. 2. (a) The steady-state photon number $|a_{1,s}|^2$ as a function of the optical detuning Δ_L. The dependence of $|a_{1,s}|^2$ on the spinning speed Ω is clearly seen. (b) The mechanical displacement amplification factor η versus Δ_L. Parameters are chosen as $\Omega = 6$ kHz, $J/\omega_m = 0.5$, and $P_{\rm in} = 10\ \mu$W.

ratio η of the steady-sate mechanical displacement x_s for spinning and not spinning the resonator is given by

$$\eta_{>,<} \equiv \frac{x_s(\Delta_{\rm Sag} > 0, < 0)}{x_s(\Omega = 0)}.$$

In close analogy to an optical laser, a coherent emission of phonons can be achieved with compound resonators through inversion of the two optical supermodes [16,17]. This leads to a *phonon laser at the breathing mode* with frequency ω_m, above the threshold power $P_{\rm th} \sim 7\ \mu$W, according to Grudinin *et al.* [16].

By use of the supermode operators $a_\pm = (a_1 \pm a_2)/\sqrt{2}$, H_0 and $H_{\rm dr}$ in Eq. (2) can be written as

$$\begin{aligned}\mathcal{H}_0 &= \omega_+ a_+^\dagger a_+ + \omega_- a_-^\dagger a_- + \omega_m b^\dagger b,\\ \mathcal{H}_{\rm dr} &= \frac{i}{\sqrt{2}}[\varepsilon_L(a_+^\dagger + a_-^\dagger) - {\rm H.c.}],\end{aligned} \tag{5}$$

with the supermode frequencies

$$\omega_{\pm} = -\Delta_L - \tfrac{1}{2}\Delta_{\mathrm{Sag}} \pm J.$$

Under the rotating-wave approximation [16,20], the interaction Hamiltonian can be written as

$$\mathcal{H}_{\mathrm{int}} = -\frac{\zeta x_0}{2}(a_+^\dagger a_- b + b^\dagger a_-^\dagger a_+) + \frac{\Delta_{\mathrm{Sag}}}{2}(a_+^\dagger a_- + a_-^\dagger a_+). \tag{6}$$

Besides the first term, which describes the absorption and emission of phonons (as in a conventional COM system) [16], $\mathcal{H}_{\mathrm{int}}$ in Eq. (6) includes an additional Ω-dependent term that implies that the *coupling* between the optical supermodes depends on the Sagnac effect. The second term in Eq. (6) is the reason for the striking modifications in the phonon-lasing process, which is very different from the ordinary cases without the coupling of supermodes [16]. In general, the supermode operators $a_{\pm} = (a_1 \pm a_2)/\sqrt{2}$ are defined for coupled cavities sharing the same resonant frequency. These operators can still be used here because the Sagnac shift in our system is much smaller than the optical detuning and the optical coupling rate. It is possible to introduce another transformation to diagonalize the two-mode system, such as that in recent work on a phonon laser [18]. We have confirmed that, since the Sagnac shift is $\Delta_{\mathrm{Sag}}/\omega_m \simeq 0.1$ for $\Omega = 6$ kHz (i.e., much smaller than Δ_L and J), this transformation can be safely reduced to the above operators as we used.

In the supermode picture, we can define the *ladder* operator and *population-inversion* operator of the optical supermodes as [16]

$$p = a_-^\dagger a_+, \quad \delta n = a_+^\dagger a_+ - a_-^\dagger a_-,$$

respectively. The equations of motion of the system then become

$$\begin{aligned}\dot{b} &= -(\gamma_m + i\omega_m)b + \frac{i\zeta x_0}{2}p,\\ \dot{p} &= -2(\gamma + iJ)p + \frac{i}{2}(\Delta_{\mathrm{Sag}} - \zeta x_0 b)\delta n\\ &\quad + \frac{1}{\sqrt{2}}(\varepsilon_L^* a_+ + \varepsilon_L a_-^\dagger),\end{aligned} \tag{7}$$

with $\gamma = (\gamma_1 + \gamma_2)/2$. By using the standard procedures (see Appendix B for more details), we can easily obtain the *mechanical gain*; that is, $G = G_0 + \mathcal{G}$, where

$$G_0 = \frac{(\zeta x_0)^2 \gamma \delta n}{2(2J - \omega_m)^2 + 8\gamma^2} \tag{8}$$

and

$$\mathcal{G} = \frac{|\varepsilon_L|^2 (\zeta x_0)^2 (\omega_m - 2J)(\Delta_{\mathrm{Sag}} + 2\Delta_L)\gamma}{4[\beta^2 + (2\Delta_L + \Delta_{\mathrm{Sag}})^2\gamma^2][(2J - \omega_m)^2 + 4\gamma^2]}, \tag{9}$$

with

$$\beta \simeq J^2 + \gamma^2 - \Delta_L^2 + \frac{(\zeta x_0)^2 n_b}{4} - \Delta_{\mathrm{Sag}}\Delta_L, \tag{10}$$

in consideration of $\Delta_{\mathrm{Sag}} \ll \Delta_L, J$ and $\zeta x_0/\Delta_L \ll 1$. The *population inversion* δn can also be derived as

$$\delta n \simeq \frac{2J|\varepsilon_L|^2}{\beta_0^2 + 4\gamma^2\Delta_L^2}(\Delta_L + \Delta_{\mathrm{Sag}}), \tag{11}$$

with $\beta_0 = \beta(\Delta_{\mathrm{Sag}} = 0)$. We have confirmed that the condition $\zeta x_0/\Delta_L \ll 1$ is valid for the range of parameters used in this work. However, in the numerical simulations, we do *not* use this approximation and thus the results presented are valid for the general case. Different from the conventional phonon-laser system, where both resonators are stationary [16], besides the term G_0, we also have a new term $\mathcal{G}$ that depends on both Δ_{Sag} and Δ_L. This indicates that by tuning Ω and Δ_L together, we can make the *mechanical gain G very different* for $\Delta_{\mathrm{Sag}} > 0$ or $\Delta_{\mathrm{Sag}} < 0$.

The non-negative mechanical gain G decreases the effective damping rate of the mechanical mode $\gamma_{\mathrm{eff}} = \gamma_m - G$. Initially, this leads to heating of the mechanical oscillator, and parametric instabilities can occur for $\gamma_{\mathrm{eff}} < 0$. In this situation, an initial fluctuation of the mechanical displacement can grow exponentially until the oscillation amplitude is saturated due to the nonlinear effects, which results in a steady-state regime with a fixed oscillation amplitude (i.e., the phonon-lasing regime) [3,16]. In practice, the in-phase and quadrature components of the mechanical motion mode, as well as its power spectral density, can be experimentally measured, from which a transition from a thermal state below threshold to a coherent state above threshold can be demonstrated, as the linear gain is turned on and allowed to increase until the phonon laser reaches the steady state [15].

III. NUMERICAL RESULTS AND DISCUSSION

Figure 2(a) shows the steady-state populations of intracavity photons as a function of the optical detuning. As in relevant experiments [16,70,80], the parameter values are taken as $n = 1.48$, $r_1 = 34.5$ μm, $Q_1 = 9.7 \times 10^7$, $r_2 = 4.75$ mm, $Q_2 = 3 \times 10^7$, $m = 50$ ng, $\gamma_m =$

0.24 MHz, $\omega_m = 2\pi \times 23.4$ MHz, and $\Omega = 6$ kHz, and thus $\Delta_{\rm Sag}/\omega_m \sim 0.1$. It is seen that spinning the resonator *increases* the intracavity photon number $|a_{1,s}|^2$ when $\Delta_{\rm Sag} > 0$ or *decreases* it when $\Delta_{\rm Sag} < 0$, compared with the stationary-resonator case ($\Omega = 0$). This change in the intracavity photon number then modifies the radiation pressure. Thus, we *can tune (increase or decrease) the strength of optomechanical interactions effectively by tuning the speed and direction of the rotation of the resonator*. Intuitively, this direction-dependent feature for the intracavity photon number (and also the resulting radiation pressure) can be well understood by the motion-induced different refractive indices for the counterpropagating modes, as demonstrated very recently in a spinning resonator [70] (see also similar phenomena in a moving optical lattice [81] or in an acoustic device with a circulating fluid [75]).

Figure 2(b) shows the mechanical displacement amplification factor η. Note that x_s is enhanced in the red-detuning regime for $\Delta_{\rm Sag} > 0$ or in the blue-detuning regime for $\Delta_{\rm Sag} < 0$, which is due to the enhanced COM interaction. The amplified displacement indicates an enhancement of phonon generation.

We show in Fig. 3 the mechanical gain G as a function of the optical detuning Δ_L for different values of Ω. In the stationary-resonator case ($\Omega = 0$), the peak position of G is always the same regardless of the direction of the driving light: we have $G > \gamma_m$ around $\Delta_L/\omega_m \sim 0.5$, corresponding to a conventional phonon laser in the blue-detuning regime [16]. In contrast, spinning of the resonator leads to a redshift or blueshift shift also for the mechanical gain G, with $\Delta_{\rm Sag} > 0$ or $\Delta_{\rm Sag} < 0$, respectively. Because of these shifts, by tuning Δ_L (e.g., $\Delta_L/\omega_m \sim 0.45$ in the specific example in Fig. 3), we can enhance the mechanical gain for $\Delta_{\rm Sag} > 0$ and significantly suppress it (i.e., $G < \gamma_m$) for $\Delta_{\rm Sag} < 0$.

The underlying physics can be explained as follows. Spinning the resonator results in opposite shifts of the counterpropagating WGMs, leading to nonreciprocal light transmission [70]. For the $\Delta_{\rm Sag} > 0$ case, the driving light is in the resonators, inducing an *enhanced radiation pressure*, which corresponds to an enhanced population inversion [see Eq. (11)]. As a result, the mechanical gain is enhanced. For the $\Delta_{\rm Sag} < 0$ case, on the other hand, the driving light is transmitted out of the resonators, inducing a weakened radiation pressure, so the mechanical gain is nearly zero, (i.e., no phonon lasing). Thus, our system provides a new route to control the behavior of phonon lasing.

Once the mechanical gain is obtained, the *stimulated emitted phonon number* N_b can be calculated; that is,

$$N_b = \exp[2(G - \gamma_m)/\gamma_m], \tag{12}$$

which characterizes the performance of the phonon laser. Figure 4(a) shows N_b with $\Delta_L/\omega_m = 0.45$ and $\Omega = 6$ kHz

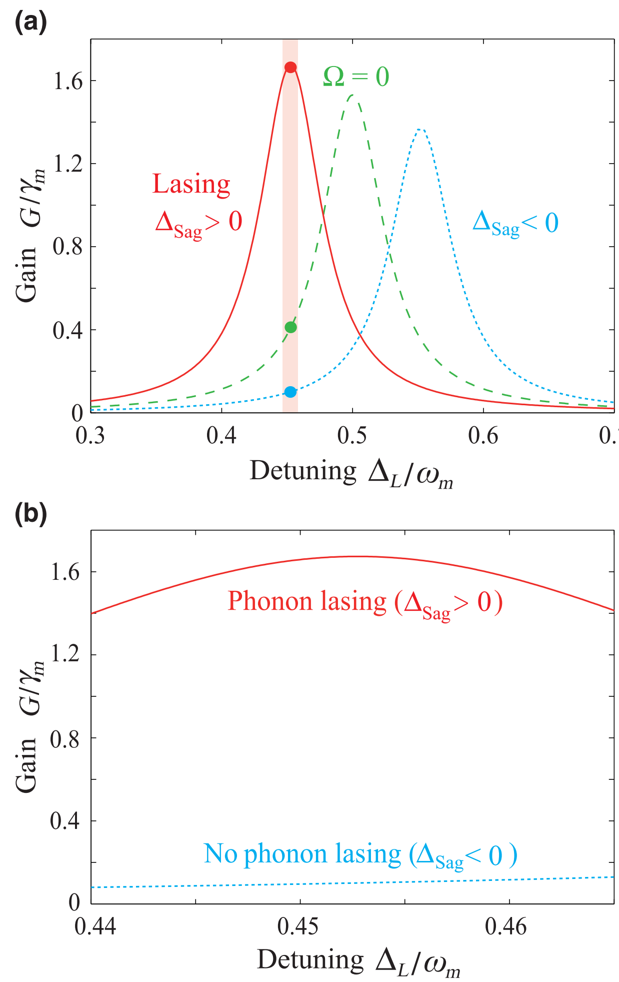

FIG. 3. (a,b) The scaled mechanical gain G/γ_m as a function of the optical detuning Δ_L. Phonon lasing can be generated (red curve) or prohibited (blue curve) for different rotation directions, indicating that acoustic nonreciprocity can be achieved, as shown in (b). The thick points in the vertical pink band in (a) correspond to two different driving directions at $\Delta_L/\omega_m = 0.45$. The other parameters are the same as those in Fig. 2.

[corresponding to the maximal value of the mechanical gain in Fig. 3(a)]. From the threshold condition for phonon lasing $N_b = 1$ (i.e., $G = \gamma_m$), we can easily derive the threshold pump power [16]. For $J/\omega_m = 0.5$, we substitute Eqs. (8) and (11) into the threshold condition, and then obtain

$$P_{\rm th} \approx \frac{2\hbar\gamma\gamma_m\omega_c[M + \gamma^2(2\Delta_L + \Delta_{\rm Sag})^2]}{\gamma_1 J(\zeta x_0)^2(\Delta_L + \Delta_{\rm Sag})}, \tag{13}$$

with

$$M = (J^2 + \gamma^2 - \Delta_L^2 - \Delta_{\rm Sag}\Delta_L)^2,$$

in which we have used $|b_s|^2 \ll 1$ at the threshold. We can see that the Sagnac effect has a significant impact

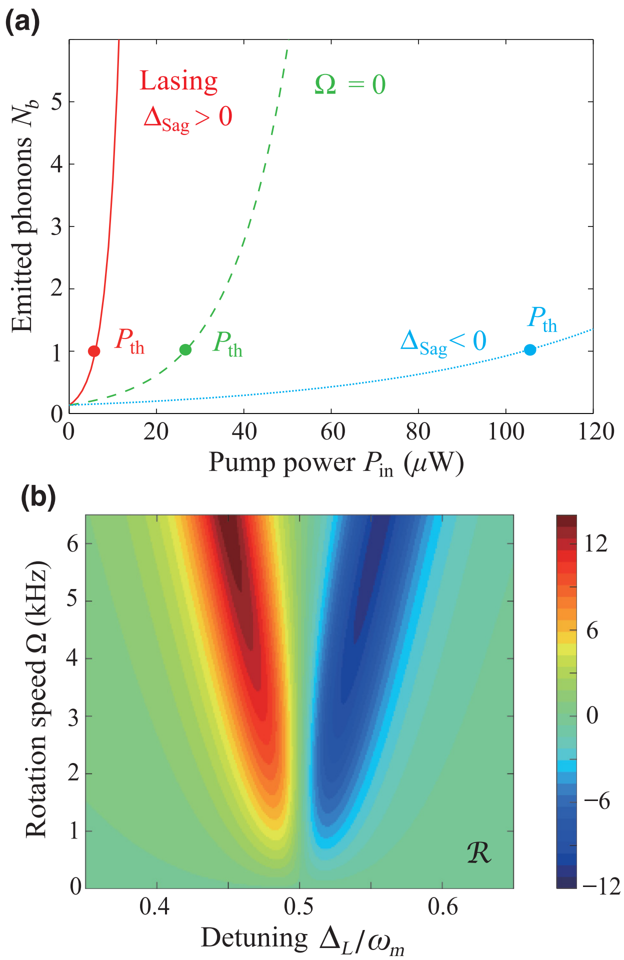

FIG. 4. (a) The stimulated emitted phonon number N_b as a function of the pump power $P_{\rm in}$. The thick points correspond to the threshold power $P_{\rm th}$, which is determined by the threshold condition $G = \gamma_m$. (b) Dependence of the isolation parameter $\mathcal{R}$ on the optical detuning Δ_L and the rotation speed Ω. The isolation parameter $\mathcal{R}$ can be maximized as $\mathcal{R} \sim 10$ dB for $\Delta_L/\omega_m = 0.45$ and $\Omega = 6$ kHz [red point in Fig. 3(a)]. The parameters are $J/\omega_m = 0.5$ in (a,b), and $P_{\rm in} = 10\ \mu$W in (b).

on the threshold. For $\Delta_{\rm Sag} > 0$, the threshold power can be reduced to 6.03 μW, which is attributed to the enhancement of the mechanical gain. It is obvious that more phonons can be generated with larger pump powers. For $\Delta_{\rm Sag} < 0$, the mechanical gain is blocked at $\Delta_L/\omega_m = 0.45$, so a larger input power is needed to achieve a phonon laser. The threshold power is up to about 26.6 μW for a stationary system ($\Omega = 0$). However, at the resonance point ($\Delta_L/\omega_m = 0.5$), the threshold for phonon lasing is 6.53 μW, which approaches the threshold of about 7 μW reported in experiments [16].

An *optimal spinning speed* should be chosen to obtain a considerable phonon number. To clearly see the effect of the spinning speed on the stimulated emitted phonon number, we introduce the isolation parameter [42,60]

$$\mathcal{R} = 10 \log_{10} \frac{N_b(\Omega > 0)}{N_b(\Omega < 0)}. \tag{14}$$

Acoustic nonreciprocity can be achieved for $\mathcal{R} \neq 0$ or

$$N_b(\Delta_{\rm Sag} > 0) \neq N_b(\Delta_{\rm Sag} < 0),$$

indicating that the spinning COM system is driven from two different directions.

Figure 4(b) shows $\mathcal{R}$ versus the optical detuning and spinning speed. Nonreciprocity emerges for the two detuning regions around $\Delta_L/\omega_m \sim 0.45$ and $\Delta_L/\omega_m \sim 0.55$. For $\Delta_L/\omega_m = 0.5$, we have $\mathcal{R} \sim 0$, implying a reciprocal system. The nonreciprocity becomes obvious for the spinning resonator, which is an inevitable result from the difference between $\delta n(\Delta_{\rm Sag} > 0)$ and $\delta n(\Delta_{\rm Sag} < 0)$. Phonon lasing is favorable in the $\Delta_{\rm Sag} > 0$ regime and is always suppressed for $\Delta_{\rm Sag} < 0$. This brings about the convenience of turning on or off the phonon lasing just by changing the driving direction. Optical nonreciprocity has been demonstrated in a pure optical system by spinning of the resonator [70]. In our spinning COM device, nonreciprocal phonon lasing can be realized due to the optical Sagnac effect, which can change the radiation pressure in the COM devices.

IV. SUMMARY

In summary, we study theoretically the role of rotation in engineering a nonreciprocal phonon laser. We show that in our system, consisting of a COM resonator coupled to a spinning optical resonator [16,70], the optical Sagnac effect strongly modifies not only the intracavity optical intensities but also the mechanical gain and the phonon-lasing threshold. As a result, the threshold pump power can be reduced or raised, depending on whether the drive is input in the same direction as or in the direction opposite that of the spinning resonator. Our results (i.e., controlling the behavior of a phonon laser by use of a spinning resonator) shed new light on engineering COM or other acoustic devices, such as COM transducers or motion sensors. In future work, we will further study, for example, purely quantum correlations of emitted phonons, in which quantum noise terms should be included, or a nonreciprocal phonon laser operating at an exceptional point [18].

ACKNOWLEDGMENTS

We thank S.K. Özdemir at Pennsylvania State University for helpful discussions. Y.J. and H.J. are supported by the National Natural Science Foundation of China (Grants No. 11474087 and No. 11774086). S.M. and T.C. are supported by the Israeli Centers of Research Excellence Circle of Light and the Israeli Science Foundation. F.N. is supported by the MURI Center for Dynamic Magneto-Optics via the Air Force Office of Scientific Research (Grant No. FA9550-14-1-0040), the Army Research Office (Grant No. 73315PH), the Asian Office of Aerospace Research and Development (Grant No. FA2386-18-1-4045), the Japan Science and Technology Agency (the ImPACT program and CREST Grant No. JPMJCR1676), the Japan Society for the Promotion of Science (JSPS-RFBR Grant No. 17-52-50023), the RIKEN-AIST Challenge Research Fund, and the John Templeton Foundation.

APPENDIX A: DERIVATION OF THE HAMILTONIAN

We consider two coupled WGM resonators, as shown in Fig. 1. One resonator supports a mechanical mode with frequency ω_m and effective mass m, which is pumped by a driving field at frequency ω_L. The other resonator is purely optical, and can spin. The optical modes in the COM and optical resonators are denoted as a_1 and a_2, respectively.

The two cavities share the same resonance frequency (denoted as ω_c) for the stationary case. The resonance frequency of the spinning optical resonator can be shifted, as a result of the Sagnac effect. Therefore, the free Hamiltonian describing the optical and mechanical modes can be written as ($\hbar = 1$)

$$H_0' = \omega_c a_1^\dagger a_1 + (\omega_c - \Delta_{\rm Sag}) a_2^\dagger a_2 + \omega_m b^\dagger b, \qquad \text{(A1)}$$

where b is the mechanical annihilation operator and $\Delta_{\rm Sag}$ is the frequency shift induced by the Sagnac effect. For the resonator spinning along the CCW direction, $\Delta_{\rm Sag} > 0$ or $\Delta_{\rm Sag} < 0$ corresponds to the driving field from the left or the right.

In this system, we consider the coupling between the optical mode and the mechanical mode in the COM resonator, and the evanescent coupling between the two resonators. The interaction Hamiltonian can be written as

$$H_{\rm int}' = -\zeta x_0 a_1^\dagger a_1 (b^\dagger + b) + J(a_1^\dagger a_2 + a_2^\dagger a_1), \qquad \text{(A2)}$$

where $\zeta = \omega_c / r_1$ denotes the COM coupling strength, J is the optical coupling strength, and $x_0 = \sqrt{\hbar/2m\omega_m}$. The driving field is fed into the COM resonator through the waveguide. Then the driving Hamiltonian reads

$$H_{\rm dr}' = i(\varepsilon_L e^{-i\omega_L t} a_1^\dagger - \varepsilon_L^* e^{i\omega_L t} a_1), \qquad \text{(A3)}$$

where $\varepsilon_L = \sqrt{2\gamma_1 P_{\rm in}/\hbar\omega_L}$ is the driving amplitude with input power $P_{\rm in}$ and optical loss rate γ_1.

The total Hamiltonian of the system can be written as

$$H' = H_0' + H_{\rm int}' + H_{\rm dr}'.$$

By using the unitary transformation

$$U = e^{-i\omega_L t (a_1^\dagger a_1 + a_2^\dagger a_2)},$$

we can transform the Hamiltonian H' into the rotating frame; that is,

$$H = U^\dagger H' U - iU^\dagger \frac{\partial U}{\partial t}.$$

Then we have

$$\begin{aligned} H &= H_0 + H_{\rm int} + H_{\rm dr}, \\ H_0 &= -\Delta_L a_1^\dagger a_1 - (\Delta_L + \Delta_{\rm Sag}) a_2^\dagger a_2 + \omega_m b^\dagger b, \\ H_{\rm int} &= -\zeta x_0 a_1^\dagger a_1 (b^\dagger + b) + J(a_1^\dagger a_2 + a_2^\dagger a_1), \\ H_{\rm dr} &= i(\varepsilon_L a_1^\dagger - \varepsilon_L^* a_1), \end{aligned} \qquad \text{(A4)}$$

where $\Delta_L = \omega_L - \omega_c$ is the detuning of the driving field. This Hamiltonian sets the stage for our calculations of the mechanical gain and the threshold power.

We then introduce the supermode operators $a_\pm = (a_1 \pm a_2)/\sqrt{2}$, which satisfy the commutation relations

$$[a_+, a_+^\dagger] = [a_-, a_-^\dagger] = 1, \quad [a_+, a_-^\dagger] = 0.$$

H_0 and $H_{\rm dr}$ in Eq. (A4) can be written as

$$\begin{aligned} \mathcal{H}_0 &= \omega_+ a_+^\dagger a_+ + \omega_- a_-^\dagger a_- + \omega_m b^\dagger b, \\ \mathcal{H}_{\rm dr} &= \frac{i}{\sqrt{2}} [\varepsilon_L (a_+^\dagger + a_-^\dagger) - \text{H.c.}], \end{aligned} \qquad \text{(A5)}$$

with the frequencies $\omega_\pm = -\Delta_L - \frac{1}{2}\Delta_{\rm Sag} \pm J$, and $H_{\rm int}$ can be transformed to

$$\begin{aligned} \mathcal{H}_{\rm int} &= \mathcal{H}_{\rm int}^0 + \mathcal{H}_{\rm int}^1 \\ &= -\frac{\zeta x_0}{2}[(a_+^\dagger a_+ + a_-^\dagger a_-) + (a_+^\dagger a_- + a_-^\dagger a_+)](b^\dagger + b) \\ &\quad + \frac{\Delta_{\rm Sag}}{2}(a_+^\dagger a_- + a_-^\dagger a_+). \end{aligned} \qquad \text{(A6)}$$

In the rotating frame with respect to $\mathcal{H}_0$, we have

$$\begin{aligned} \mathcal{H}_{\rm int}^0 = -\frac{\zeta x_0}{2}[& a_+^\dagger a_- b \mathrm{e}^{i(2J-\omega_m)t} + a_+ a_-^\dagger b^\dagger \mathrm{e}^{-i(2J-\omega_m)t} \\ & + a_+^\dagger a_- b^\dagger \mathrm{e}^{i(2J+\omega_m)t} + a_+ a_-^\dagger b \mathrm{e}^{-i(2J+\omega_m)t} \\ & + (a_+^\dagger a_+ + a_-^\dagger a_-)(b^\dagger \mathrm{e}^{i\omega_m t} + b \mathrm{e}^{-i\omega_m t})]. \end{aligned}$$

Under the rotating-wave-approximation condition

$$2J + \omega_m, \quad \omega_m \gg |2J - \omega_m|,$$

the terms $a_+^\dagger a_- b^\dagger \mathrm{e}^{i(2J+\omega_m)t}$, $a_+ a_-^\dagger b \mathrm{e}^{-i(2J+\omega_m)t}$, and $(a_+^\dagger a_+ + a_-^\dagger a_-)(b^\dagger \mathrm{e}^{i\omega_m t} + b\mathrm{e}^{-i\omega_m t})$ can be omitted in comparison with the near-resonance terms $a_+^\dagger a_- b \mathrm{e}^{i(2J-\omega_m)t}$ and

$a_+a_-^\dagger b^\dagger e^{-i(2J-\omega_m)t}$ [16]. Therefore, we have a simplified interaction Hamiltonian:

$$\mathcal{H}_{\rm int} = -\frac{\zeta x_0}{2}(a_+^\dagger a_- b + b^\dagger a_-^\dagger a_+) + \frac{\Delta_{\rm Sag}}{2}(a_+^\dagger a_- + a_-^\dagger a_+). \tag{A7}$$

APPENDIX B: DERIVATION OF THE MECHANICAL GAIN

In the supermode picture, the equations of motion of the system can be written as

$$\begin{aligned}\dot{a}_+ &= -(i\omega_+ + \gamma)a_+ + \frac{i}{2}(\zeta x_0 b - \Delta_{\rm Sag})a_- + \frac{\varepsilon_L}{\sqrt{2}},\\ \dot{a}_- &= -(i\omega_- + \gamma)a_- + \frac{i}{2}(\zeta x_0 b^\dagger - \Delta_{\rm Sag})a_+ + \frac{\varepsilon_L}{\sqrt{2}},\\ \dot{b} &= -(i\omega_m + \gamma_m)b + \frac{i\zeta x_0}{2}a_+ a_-^\dagger.\end{aligned} \tag{B1}$$

We can define the ladder operator and the population-inversion operator as

$$p = a_-^\dagger a_+, \quad \delta n = a_+^\dagger a_+ - a_-^\dagger a_-,$$

respectively. The equations of the system then read

$$\begin{aligned}\dot{b} &= -(\gamma_m + i\omega_m)b + \frac{i\zeta x_0}{2}p,\\ \dot{p} &= -2(\gamma + iJ)p + \frac{i}{2}(\Delta_{\rm Sag} - \zeta x_0 b)\delta n\\ &\quad + \frac{1}{\sqrt{2}}(\varepsilon_L^* a_+ + \varepsilon_L a_-^\dagger).\end{aligned} \tag{B2}$$

By setting the time derivatives of $a_\pm$ and p to zero with $\gamma \gg \gamma_m$, we obtain the steady-state values of the system; that is,

$$\begin{aligned}p &= \frac{\sqrt{2}(\varepsilon_L^* a_+ + \varepsilon_L a_-^\dagger) - i(\zeta x_0 b - \Delta_{\rm Sag})\delta n}{2i(2J-\omega_m) + 4\gamma},\\ a_+ &= \frac{\varepsilon_L(2i\omega_- + 2\gamma + i\zeta x_0 b - i\Delta_{\rm Sag})}{2\sqrt{2}[\beta - i(2\Delta_L + \Delta_{\rm Sag})\gamma]},\\ a_- &= \frac{\varepsilon_L(2i\omega_+ + 2\gamma + i\zeta x_0 b^\dagger - i\Delta_{\rm Sag})}{2\sqrt{2}[\beta - i(2\Delta_L + \Delta_{\rm Sag})\gamma]},\end{aligned} \tag{B3}$$

with

$$\beta = \beta_0 - \Delta_{\rm Sag}\left[\Delta_L + \frac{\zeta x_0}{2}{\rm Re}(b)\right],$$

$$\beta_0 = J^2 + \gamma^2 - \Delta_L^2 + \frac{(\zeta x_0)^2 n_b}{4},$$

where the phonon number $n_b = b^\dagger b$. Substitution of Eq. (B3) into the dynamical equation of b in Eq. (B2) results in

$$\dot{b} = (-i\omega_m - i\omega' + G - \gamma_m)b + D, \tag{B4}$$

where

$$\begin{aligned}\omega' &= \frac{(\zeta x_0)^2(2J-\omega_m)\delta n}{4(2J-\omega_m)^2 + 16\gamma^2}\\ &\quad + \frac{(\zeta x_0)^2|\varepsilon_L|^2\gamma^2(2\Delta_L + \Delta_{\rm Sag})}{[2(2J-\omega_m)^2 + 8\gamma^2][\beta^2 + (2\Delta_L + \Delta_{\rm Sag})^2\gamma^2]},\\ D &= \frac{\zeta x_0 \Delta_{\rm Sag}\delta n}{4i(2J-\omega_m) + 8\gamma}\\ &\quad + \frac{i\zeta x_0 \beta(\gamma - iJ)|\varepsilon_L|^2}{[2i(2J-\omega_m) + 4\gamma][\beta^2 + (2\Delta_L + \Delta_{\rm Sag})^2\gamma^2]}\\ &\quad + \frac{i\zeta x_0 \gamma|\varepsilon_L|^2(2\Delta_L + \Delta_{\rm Sag})(\Delta_L + \Delta_{\rm Sag})}{[2i(2J-\omega_m) + 4\gamma][\beta^2 + (2\Delta_L + \Delta_{\rm Sag})^2\gamma^2]},\end{aligned}$$

and the mechanical gain is $G = G_0 + \mathcal{G}$, with

$$\begin{aligned}G_0 &= \frac{(\zeta x_0)^2\gamma\delta n}{2(2J-\omega_m)^2 + 8\gamma^2},\\ \mathcal{G} &= \frac{|\varepsilon_L|^2(\zeta x_0)^2(\omega_m - 2J)(\Delta_{\rm Sag} + 2\Delta_L)\gamma}{4[\beta^2 + (2\Delta_L + \Delta_{\rm Sag})^2\gamma^2][(2J-\omega_m)^2 + 4\gamma^2]},\end{aligned} \tag{B5}$$

where δn can be expressed as

$$\delta n = \frac{|\varepsilon_L|^2[2J(\Delta_L + \Delta_{\rm Sag}) - \gamma\zeta x_0{\rm Im}(b) - J\zeta x_0{\rm Re}(b)]}{\beta^2 + \gamma^2(2\Delta_L + \Delta_{\rm Sag})^2}.$$

In consideration of $\Delta_{\rm Sag} \ll \Delta_L, J$ and $\zeta x_0/\Delta_L \ll 1$, we have

$$\begin{aligned}\delta n &\simeq \frac{|\varepsilon_L|^2[2J(\Delta_L + \Delta_{\rm Sag}) - \gamma\zeta x_0\,{\rm Im}(b) - J\zeta x_0\,{\rm Re}(b)]}{\beta_0^2 + 4\gamma^2\Delta_L(\Delta_L - \Delta_{\rm Sag}) + \beta_0\Delta_{\rm Sag}[\Delta_L + \zeta x_0\,{\rm Re}(b)]}\\ &\simeq |\varepsilon_L|^2\cdot\frac{2J\Delta_L - \gamma\zeta x_0\,{\rm Im}(b) - J\zeta x_0\,{\rm Re}(b) - 2J\Delta_{\rm Sag}}{\beta_0^2 + 4\gamma^2\Delta_L^2}\\ &\quad \cdot\left[1 - \frac{\beta_0\Delta_{\rm Sag}(2\Delta_L + \zeta x_0\,{\rm Re}(b)) - 8\gamma^2\Delta_L\Delta_{\rm Sag}}{\beta_0^2 + 4\gamma^2\Delta_L^2}\right]\\ &\simeq \frac{|\varepsilon_L|^2[2J\Delta_L - J\zeta x_0\,{\rm Re}(b) - \gamma\zeta x_0\,{\rm Im}(b)]}{\beta_0^2 + 4\gamma^2\Delta_L^2}\end{aligned}$$

$$\cdot \left(1 + \frac{2\Delta_{\mathrm{Sag}}\beta_0\Delta_L}{\beta_0^2 + 4\gamma^2\Delta_L^2}\right) + \frac{2\Delta_{\mathrm{Sag}}J|\varepsilon_L|^2}{\beta_0^2 + 4\gamma^2\Delta_L^2}$$
$$\simeq \frac{2J|\varepsilon_L|^2}{\beta_0^2 + 4\gamma^2\Delta_L^2}(\Delta_L + \Delta_{\mathrm{Sag}}),$$

in which we have used $\beta \simeq \beta_0 - \Delta_{\mathrm{Sag}}\Delta_L$.

APPENDIX C: EXPERIMENTAL FEASIBILITY OF THE SPINNING RESONATOR

The resonator can be mounted on a turbine, which spins the resonator, as in a very recent experiment [70]. In this experiment, the resonator with radius $r = 4.75$ mm can spin with the stability of its axis, reaching a rotation frequency of 3 kHz. In our calculations, the rotation speed is chosen according to this experiment [70]. For example, the Sagnac shift is $\Delta_{\mathrm{Sag}} = 14.6$ MHz for $\Omega = 6$ kHz, leading to $\Delta_{\mathrm{Sag}}/\omega_m \sim 0.1$.

By positioning the resonator near a single-mode fiber, we can couple the light into or out the resonator evanescently through the tapered region. In the device, aerodynamic processes lead to a stable resonator-fiber coupling, which can be explained as follows. A fast-spinning resonator can drag air into the region between the cavity and the taper, forming a boundary layer of air. Because of the air pressure on the surface of the taper facing the resonator, the taper flies at a height above the resonator, which can be several nanometers. If some perturbation causes the taper to rise higher than the stable equilibrium height, it floats back to its original position [70]. The self-adjustment of the taper separation from the spinning resonator enables critical coupling of light into the cavity, by which counter-circulating lights experience optical drags identical in size but opposite in sign. This experiment also confirms that the taper does not touch or stick to the rotating resonator even if the taper is pushed toward it, which is in contrast to the situation for a stationary resonator (i.e., the taper can stick to the resonator through van der Waals forces and thus needs to be pulled back to break the connection). Other factors, including intermolecular forces, lubricant compressibility, tapered-fiber stiffness, and the wrap angle of the fiber, may affect the resonator-waveguide coupling. However, these factors are confirmed to be negligible in the experiment. In our scheme, the spinning resonator is coupled with the stationary COM resonator, instead of the fiber, in which stationary coupling of the two resonators can also be achieved.

[1] P. Meystre, A short walk through quantum optomechanics, Ann. Phys. (Berlin) **525**, 215 (2013).

[2] M. Metcalfe, Applications of cavity optomechanics, Appl. Phys. Rev. **1**, 031105 (2014).

[3] M. Aspelmeyer, T. J. Kippenberg, and F. Marquardt, Cavity optomechanics, Rev. Mod. Phys. **86**, 1391 (2014).

[4] M. Bagheri, M. Poot, M. Li, W. P. H. Pernice, and H. X. Tang, Dynamic manipulation of nanomechanical resonators in the high-amplitude regime and non-volatile mechanical memory operation, Nat. Nanotechnol. **6**, 726 (2011).

[5] T. Bagci, A. Simonsen, S. Schmid, L. G. Villanueva, E. Zeuthen, J. Appel, J. M. Taylor, A. Sørensen, K. Usami, A. Schliesser, and E. S. Polzik, Optical detection of radio waves through a nanomechanical transducer, Nature (London) **507**, 81 (2014).

[6] L. Tian, Optoelectromechanical transducer: Reversible conversion between microwave and optical photons, Ann. Phys. (Berlin) **527**, 1 (2015).

[7] F. Lecocq, J. B. Clark, R. W. Simmonds, J. Aumentado, and J. D. Teufel, Mechanically Mediated Microwave Frequency Conversion in the Quantum Regime, Phys. Rev. Lett. **116**, 043601 (2016).

[8] O. Arcizet, P.-F. Cohadon, T. Briant, M. Pinard, A. Heidmann, J.-M. Mackowski, C. Michel, L. Pinard, O. Français, and L. Rousseau, High-Sensitivity Optical Monitoring of a Micromechanical Resonator with a Quantum-Limited Optomechanical Sensor, Phys. Rev. Lett. **97**, 133601 (2006).

[9] K. Srinivasan, H. Miao, M. T. Rakher, M. Davanço, and V. Aksyuk, Optomechanical Transduction of an Integrated Silicon Cantilever Probe Using a Microdisk Resonator, Nano Lett. **11**, 791 (2011).

[10] F. Monifi, J. Zhang, Ş. K. Özdemir, B. Peng, Y.-X. Liu, F. Bo, F. Nori, and L. Yang, Optomechanically induced stochastic resonance and chaos transfer between optical fields, Nat. Photon. **10**, 399 (2016).

[11] K. Vahala, M. Herrmann, S. Knünz, V. Batteiger, G. Saathoff, T. W. Hänsch, and T. Udem, A phonon laser, Nat. Phys. **5**, 682 (2009).

[12] R. P. Beardsley, A. V. Akimov, M. Henini, and A. J. Kent, Coherent Terahertz Sound Amplification and Spectral Line Narrowing in a Stark Ladder Superlattice, Phys. Rev. Lett. **104**, 085501 (2010).

[13] I. Mahboob, K. Nishiguchi, A. Fujiwara, and H. Yamaguchi, Phonon Lasing in an Electromechanical Resonator, Phys. Rev. Lett. **110**, 127202 (2013).

[14] U. Kemiktarak, M. Durand, M. Metcalfe, and J. Lawall, Mode Competition and Anomalous Cooling in a Multimode Phonon Laser, Phys. Rev. Lett. **113**, 030802 (2014).

[15] J. D. Cohen, S. M. Meenehan, G. S. MacCabe, S. Gröblacher, A. H. Safavi-Naeini, F. Marsili, M. D. Shaw, and O. Painter, Phonon counting and intensity interferometry of a nanomechanical resonator, Nature (London) **520**, 522 (2015).

[16] I. S. Grudinin, H. Lee, O. Painter, and K. J. Vahala, Phonon Laser Action in a Tunable Two-Level System, Phys. Rev. Lett. **104**, 083901 (2010).

[17] G. Wang, M. Zhao, Y. Qin, Z. Yin, X. Jiang, and M. Xiao, Demonstration of an ultra-low-threshold phonon laser with coupled microtoroid resonators in vacuum, Photon. Res. **5**, 73 (2017).

[18] J. Zhang, B. Peng, Ş. K. Özdemir, K. Pichler, D. O. Krimer, G. Zhao, F. Nori, Y.-X. Liu, S. Rotter, and L. Yang, A phonon laser operating at an exceptional point, Nat. Photon. **12**, 479 (2018).

[19] H. Wu, G. Heinrich, and F. Marquardt, The effect of Landau-Zener dynamics on phonon lasing, New J. Phys. **15**, 123022 (2013).
[20] H. Jing, S. K. Özdemir, X.-Y. Lü, J. Zhang, L. Yang, and F. Nori, PT-Symmetric Phonon Laser, Phys. Rev. Lett. **113**, 053604 (2014).
[21] H. Wang, Z. Wang, J. Zhang, Ş. K. Özdemir, L. Yang, and Y. X. Liu, Phonon amplification in two coupled cavities containing one mechanical resonator, Phys. Rev. A **90**, 053814 (2014).
[22] H. Lü, S. K. Özdemir, L.-M. Kuang, F. Nori, and H. Jing, Exceptional Points in Random-Defect Phonon Lasers, Phys. Rev. Appl. **8**, 044020 (2017).
[23] L. J. Swenson, A. Cruciani, A. Benoit, M. Roesch, C. S. Yung, A. Bideaud, and A. Monfardini, High-speed phonon imaging using frequency-multiplexed kinetic inductance detectors, Appl. Phys. Lett. **96**, 263511 (2010).
[24] H. Shin, J. A. Cox, R. Jarecki, A. Starbuck, Z. Wang, and P. T. Rakich, Control of coherent information via on-chip photonic-phononic emitter-receivers, Nat. Commun. **6**, 6427 (2015).
[25] A. Ganesan, C. Do, and A. Seshia, Phononic Frequency Comb via Intrinsic Three-Wave Mixing, Phys. Rev. Lett. **118**, 033903 (2017).
[26] M. Serra-Garcia, V. Peri, R. Süsstrunk, O. R. Bilal, T. Larsen, L. G. Villanueva, and S. D. Huber, Observation of a phononic quadrupole topological insulator, Nature (London) **555**, 342 (2018).
[27] N. Li, J. Ren, L. Wang, G. Zhang, P. Hänggi, and B. Li, Phononics: Manipulating heat flow with electronic analogs and beyond, Rev. Mod. Phys. **84**, 1045 (2012).
[28] R. J. Potton, Reciprocity in optics, Rep. Prog. Phys. **67**, 717 (2004).
[29] P. Lodahl, S. Mahmoodian, S. Stobbe, A. Rauschenbeutel, P. Schneeweiss, J. Volz, H. Pichler, and P. Zoller, Chiral quantum optics, Nature (London) **541**, 473 (2017).
[30] Z. Lin, H. Ramezani, T. Eichelkraut, T. Kottos, H. Cao, and D. N. Christodoulides, Unidirectional Invisibility Induced by PT-Symmetric Periodic Structures, Phys. Rev. Lett. **106**, 213901 (2011).
[31] L. Feng, M. Ayache, J. Huang, Y.-L. Xu, M.-H. Lu, Y.-F. Chen, Y. Fainman, and A. Scherer, Nonreciprocal Light Propagation in a Silicon Photonic Circuit, Science **333**, 729 (2011).
[32] M. Scheucher, A. Hilico, E. Will, J. Volz, and A. Rauschenbeutel, Quantum optical circulator controlled by a single chirally coupled atom, Science **354**, 1577 (2016).
[33] M.-A. Miri, F. Ruesink, E. Verhagen, and A. Alù, Optical Nonreciprocity Based on Optomechanical Coupling, Phys. Rev. Appl. **7**, 064014 (2017).
[34] D. L. Sounas, and A. Alù, Non-reciprocal photonics based on time modulation, Nat. Photon. **11**, 774 (2017).
[35] B. Bahari, A. Ndao, F. Vallini, A. E. Amili, Y. Fainman, and B. Kanté, Nonreciprocal lasing in topological cavities of arbitrary geometries, Science **358**, 636 (2017).
[36] L. Bi, J. Hu, P. Jiang, D. H. Kim, G. F. Dionne, L. C. Kimerling, and C. A. Ross, On-chip optical isolation in monolithically integrated non-reciprocal optical resonators, Nat. Photon. **5**, 758 (2011).
[37] B. Peng, Ş. K. Özdemir, F. Lei, F. Monifi, M. Gianfreda, G. L. Long, S. Fan, F. Nori, C. M. Bender, and L. Yang, Parity-time-symmetric whispering-gallery microcavities, Nat. Phys. **10**, 394 (2014).
[38] L. Chang, X. Jiang, S. Hua, C. Yang, J. Wen, L. Jiang, G. Li, G. Wang, and M. Xiao, Parity-time symmetry and variable optical isolation in active-passive-coupled microresonators, Nat. Photon. **8**, 524 (2014).
[39] Y. Shi, Z. Yu, and S. Fan, Limitations of nonlinear optical isolators due to dynamic reciprocity, Nat. Photon. **9**, 388 (2015).
[40] Z. Shen, Y. L. Zhang, Y. Chen, C. L. Zou, Y. F. Xiao, X. B. Zou, F. W. Sun, G. C. Guo, and C. H. Dong, Experimental realization of optomechanically induced non-reciprocity, Nat. Photon. **10**, 657 (2016).
[41] F. Ruesink, M.-A. Miri, A. Alù, and E. Verhagen, Nonreciprocity and magnetic-free isolation based on optomechanical interactions, Nat. Commun. **7**, 13662 (2016).
[42] S. Hua, J. Wen, X. Jiang, Q. Hua, L. Jiang, and M. Xiao, Demonstration of a chip-based optical isolator with parametric amplification, Nat. Commun. **7**, 13657 (2016).
[43] K. Fang, J. Luo, A. Metelmann, M. H. Matheny, F. Marquardt, A. A. Clerk, and O. Painter, Generalized non-reciprocity in an optomechanical circuit via synthetic magnetism and reservoir engineering, Nat. Phys. **13**, 465 (2017).
[44] B. Abdo, K. Sliwa, S. Shankar, M. Hatridge, L. Frunzio, R. Schoelkopf, and M. Devoret, Josephson Directional Amplifier for Quantum Measurement of Superconducting Circuits, Phys. Rev. Lett. **112**, 167701 (2014).
[45] B. Abdo, K. Sliwa, L. Frunzio, and M. Devoret, Directional Amplification with a Josephson Circuit, Phys. Rev. X **3**, 031001 (2013).
[46] T. T. Koutserimpas, and R. Fleury, Nonreciprocal Gain in Non-Hermitian Time-Floquet Systems, Phys. Rev. Lett. **120**, 087401 (2018).
[47] Z. Shen, Y.-L. Zhang, Y. Chen, F.-W. Sun, X.-B. Zou, G.-C. Guo, C.-L. Zou, and C.-H. Dong, Reconfigurable optomechanical circulator and directional amplifier, Nat. Commun. **9**, 1797 (2018).
[48] A. Metelmann, and A. A. Clerk, Nonreciprocal Photon Transmission and Amplification via Reservoir Engineering, Phys. Rev. X **5**, 021025 (2015).
[49] A. Kamal, and A. Metelmann, Minimal Models for Nonreciprocal Amplification Using Biharmonic Drives, Phys. Rev. Appl. **7**, 034031 (2017).
[50] L. M. de Lépinay, E. Damskägg, C. F. Ockeloen-Korppi, and M. A. Sillanpää, Realization of directional amplification in a microwave optomechanical device, arXiv:1811.06036.
[51] S. Manipatruni, J. T. Robinson, and M. Lipson, Optical Nonreciprocity in Optomechanical Structures, Phys. Rev. Lett. **102**, 213903 (2009).
[52] L. D. Bino, J. M. Silver, M. T. M. Woodley, S. L. Stebbings, X. Zhao, and P. Del'Haye, Microresonator isolators and circulators based on the intrinsic nonreciprocity of the Kerr effect, Optica **5**, 279 (2018).
[53] X. Z. Zhang, L. Tian, and Y. Li, Optomechanical transistor with mechanical gain, Phys. Rev. A **97**, 043818 (2018).

[54] B. He, L. Yang, X. Jiang, and M. Xiao, Transmission Nonreciprocity in a Mutually Coupled Circulating Structure, Phys. Rev. Lett. **120**, 203904 (2018).
[55] A. Y. Song, Y. Shi, Q. Lin, and S. Fan, Direction-Dependent Parity-Time Phase Transition and Non-Reciprocal Directional Amplification with Dynamic Gain-Loss Modulation, arXiv:1806.00544.
[56] A. Metelmann, and A. A. Clerk, Nonreciprocal quantum interactions and devices via autonomous feedforward, Phys. Rev. A **95**, 013837 (2017).
[57] X.-F. Li, X. Ni, L. Feng, M.-H. Lu, C. He, and Y.-F. Chen, Tunable Unidirectional Sound Propagation through a Sonic-Crystal-Based Acoustic Diode, Phys. Rev. Lett. **106**, 084301 (2011).
[58] J. Kim, M. C. Kuzyk, K. Han, H. Wang, and G. Bahl, Nonreciprocal Brillouin scattering induced transparency, Nat. Phys. **11**, 275 (2015).
[59] R. Fleury, A. B. Khanikaev, and A. Alù, Floquet topological insulators for sound, Nat. Commun. **7**, 11744 (2016).
[60] C. Coulais, D. Sounas, and A. Alù, Static non-reciprocity in mechanical metamaterials, Nature (London) **542**, 461 (2017).
[61] A. V. Poshakinskiy, and A. N. Poddubny, Phonoritonic Crystals with a Synthetic Magnetic Field for an Acoustic Diode, Phys. Rev. Lett. **118**, 156801 (2017).
[62] S. Kim, X. Xu, J. M. Taylor, and G. Bahl, Dynamically induced robust phonon transport and chiral cooling in an optomechanical system, Nat. Commun. **8**, 205 (2017).
[63] X. Xu, S. Kim, G. Bahl, and J. M. Taylor, A quasi-mode theory of chiral phonons, arXiv:1612.09240.
[64] X. Xu, and J. M. Taylor, Optomechanically-induced chiral transport of phonons in one dimension, arXiv:1701.02699.
[65] A. Seif, W. DeGottardi, K. Esfarjani, and M. Hafezi, Thermal management and non-reciprocal control of phonon flow via optomechanics, Nat. Commun. **9**, 1207 (2018).
[66] Y. Wang, B. Yousefzadeh, H. Chen, H. Nassar, G. Huang, and C. Daraio, Observation of Nonreciprocal Wave Propagation in a Dynamic Phononic Lattice, Phys. Rev. Lett. **121**, 194301 (2018).
[67] E. J. Post, Sagnac Effect, Rev. Mod. Phys. **39**, 475 (1967).
[68] W. W. Chow, J. Gea-Banacloche, L. M. Pedrotti, V. E. Sanders, W. Schleich, and M. O. Scully, The ring laser gyro, Rev. Mod. Phys. **57**, 61 (1985).
[69] C. Ciminelli, F. Dell'Olio, C. E. Campanella, and M. N. Armenise, Photonic technologies for angular velocity sensing, Adv. Opt. Photon. **2**, 370 (2010).
[70] S. Maayani, R. Dahan, Y. Kligerman, E. Moses, A. U. Hassan, H. Jing, F. Nori, D. N. Christodoulides, and T. Carmon, Flying couplers above spinning resonators generate irreversible refraction, Nature (London) **558**, 569 (2018).
[71] L. Ge, R. Sarma, and H. Cao, Rotation-induced mode coupling in open wavelength-scale microcavities, Phys. Rev. A **90**, 013809 (2014).
[72] R. Sarma, L. Ge, J. Wiersig, and H. Cao, Rotating Optical Microcavities with Broken Chiral Symmetry, Phys. Rev. Lett. **114**, 053903 (2015).
[73] H. Jing, H. Lü, S. K. Özdemir, T. Carmon, and F. Nori, Nanoparticle sensing with a spinning resonator, Optica **5**, 1424 (2018).
[74] R. Huang, A. Miranowicz, J.-Q. Liao, F. Nori, and H. Jing, Nonreciprocal Photon Blockade, Phys. Rev. Lett. **121**, 153601 (2018).
[75] R. Fleury, D. L. Sounas, C. F. Sieck, M. R. Haberman, and A. Alù, Sound Isolation and Giant Linear Nonreciprocity in a Compact Acoustic Circulator, Science **343**, 516 (2014).
[76] H. Zhu, J. Yi, M.-Y. Li, J. Xiao, L. Zhang, C.-W. Yang, R. A. Kaindl, L.-J. Li, Y. Wang, and X. Zhang, Observation of chiral phonons, Science **359**, 579 (2018).
[77] M. C. Kuzyk, and H. Wang, Scaling Phononic Quantum Networks of Solid-State Spins with Closed Mechanical Subsystems, Phys. Rev. X **8**, 041027 (2018).
[78] G. B. Malykin, The Sagnac effect: correct and incorrect explanations, Phys. Usp. **43**, 1229 (2000).
[79] H. Lü, Y. Jiang, Y.-Z. Wang, and H. Jing, Optomechanically induced transparency in a spinning resonator, Photon. Res. **5**, 367 (2017).
[80] G. C. Righini, Y. Dumeige, P. Féron, M. Ferrari, G. N. Conti, D. Ristic, and S. Soria, Whispering gallery mode microresonators: Fundamentals and applications, Riv. Nuovo Cimento **34**, 435 (2011).
[81] H. Ramezani, P. K. Jha, Y. Wang, and X. Zhang, Nonreciprocal Localization of Photons, Phys. Rev. Lett. **120**, 043901 (2018).